ARTICLE

Electrowetting on Paper for Electronic Paper Display

Duk Young Kim and Andrew J. Steckl*

Nanoelectronics Laboratory, Department of Electrical and Computer Engineering, University of Cincinnati, Cincinnati, Ohio 45221-0030, United States

ABSTRACT The use of paper as a material for various device applications (such as microfluidics and energy storage) is very attractive given its flexibility, versatility, and low cost. Here we demonstrate that electrowetting (EW) devices can be readily fabricated on paper substrates. Several categories of paper have been investigated for this purpose, with the surface coating, roughness, thickness, and water uptake, among the most important properties. The critical parameter for EW devices is the water contact angle (CA) change with applied voltage. EW devices on paper exhibit characteristics very close to those of conventional EW devices on glass substrates. This includes a large CA change in oil ambient (90−95°), negligible hysteresis (~2°), and fast switching times of ~20 ms. These results indicate the promise of low-cost paper-based EW devices for video rate flexible e-paper on paper.

KEYWORDS: e-paper • electrowetting • paper • contact angle • fluoropolymer

I. INTRODUCTION

The quest for increasing low-cost availability of a variety of devices is directing attention to a material that has been in widespread use for centuries, namely, paper. Paper has myriad applications in everyday usage, including writing, printing, packaging, cleaning, and banknotes. The main ingredient in paper is cellulose (polysaccharide polymers) obtained by various processes from wood pulp or cotton. Paper is a layered random network of cellulose fibers of varying fiber length, diameter, and density. The penetration of water and other fluids into paper depends on the fiber surface energy, sheet structure, and porosity. Many surface coatings have been developed to modify the wetting properties of paper (1). Recently, there has been a growing interest in using paper as the substrate material for a series of devices. The attractive properties of paper as a substrate material are its wide availability in many formulations, flexibility, low cost, biosynthesis, and biodegradability. For example, the capillary property of paper can be used to transport liquids in biofluidic devices built on paper substrates (2, 3) without the need for pressure pumps or other external driving forces. In general, this is an elegant method for reducing device complexity and cost, resulting in one-time-use devices that can be totally disposed after use (by incineration). The capillary approach was used to demonstrate (4) simple fluidic switches on paper coated with a hydrophobic layer. Paper has also been used in energy storage applications as a substrate for cellulose-fiber-based batteries with good charging rates and cycling stability (5). A simple disposable device was fabricated on paper (6) using the thermochromic effect to the display temperature. The integration of paper-based products with electronics and displays is growing rapidly in the packaging industry, especially for pharmaceutical products (7).

Building on the explosive growth in "electronic paper"-based reader devices, there is a very large effort to develop e-paper displays. The current leading e-paper technology is based on electrophoretic (EPh) displays (8, 9). However, other technologies are also being investigated because EPh displays are fundamentally monochrome and do not have the speed required for video display (10).

This article reports on the use of paper as the substrate for the formation of displays based on the effect of electric fields on the wetting of solids, the so-called electrowetting (EW) effect. One of the main goals of e-paper is to replicate the look-and-feel of actual ink-on-paper. We have, therefore, investigated the use of paper as the perfect substrate for EW devices to accomplish *e-paper on paper*. The motion of liquids caused by the EW effect was recognized early on by Beni and Hackwood (11) to have very attractive characteristics for display applications: fast response time, operation with low voltage, and low power consumption. More recent EW structures utilize the voltage-induced contact angle (CA) change of an aqueous electrolyte droplet placed on the surface of a hydrophobic fluoropolymer layer and surrounded by oil (12−16). Insulating, nonpolar oils (usually alkanes) are used for this purpose because they (unlike water) do not respond directly to the applied electric field. EW technology is used in many applications (17), including reflective (18−20) and emissive (21) displays, liquid lenses (22−25), liquid-state transistors (26), and bio/medical assays (27, 28).

2. EXPERIMENTAL DETAILS

A diagram of the EW structure on a completely rolled-paper substrate and a demonstration of its EW operation are shown in Figure 1. The EW structure is built on glassine paper and consists of a ground electrode, a dielectric layer, and a fluoropolymer top layer (Figure 1b). Figure 1a shows three deion-

* To whom correspondence should be addressed. E-mail: a.steckl@uc.edu.
Received for review August 18, 2010 and accepted October 8, 2010

DOI: 10.1021/am100757g

Published on Web 10/25/2010

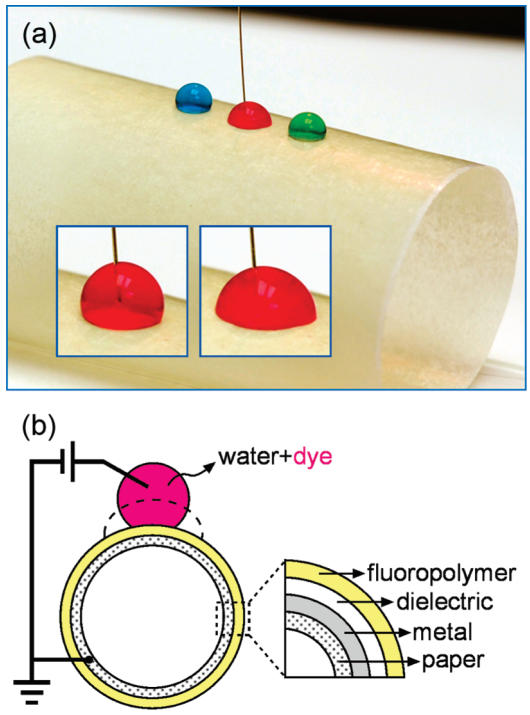

FIGURE 1. EW effect on a paper substrate: (a) photographs illustrating the EW demonstration on a rolled-paper substrate [insets show the CA change with applied voltage (right) and at zero bias (left)]; (b) diagram of the EW structure and its effect on a rolled-paper substrate.

Table 1. Properties of Glassine, Kromekote, and Sappi Papers

	glassine	Kromekote	Sappi
thickness (μm)	45	235	180
basis weight (g/m^2)	48	212	167
specific volume (m^3/g)	9.37×10^{-7}	1.11×10^{-6}	1.08×10^{-6}
water CA (deg)	44.5	80.4	105.7

ized (DI) water droplets placed on a rolled-paper EW device. The droplets contain water-soluble dyes for visualization purposes. The left (blue) and right (green) droplets show the high CA typical of aqueous droplets on hydrophobic surfaces. A wire is inserted into the middle (red) droplet, through which external voltage is applied. The EW effect results in the observable change in the CA. The insets in Figure 1a allow easy observation of the shape of the red droplet with applied voltage (right) and at zero bias (left).

Three selections of papers were found most suitable (based on the requirement of the fabrication process) as substrates for EW structures: glassine paper, Kromekote paper (10 point C1S glass white, Mohawk Fine Papers), and Sappi paper (Sappi Ltd.). Glassine paper is very thin (45 μm) and smooth, is air- and water-resistant, and is commonly used for weighing or interleaving paper. Kromekote paper is relatively thick (235 μm) and is used for annual reports, book covers, calendars, etc. Sappi paper is moderately thick (180 μm), with an ultrasmooth and hydrophobic surface. The main properties of glassine, Kromekote, and Sappi papers are summarized in Table 1.

Copper electrodes of 200 nm thickness were deposited on the paper substrates by sputtering (DV-602, Denton Vacuum) in argon at 3.5 mTorr (base pressure of 2.0×10^{-6} Torr) with 150 W radio-frequency power for 10 min. Alternatively, 200-nm-thick indium–tin oxide (ITO) electrodes were sputtered in Ar/O_2 at 3.5 mTorr with 100 W direct-current (dc) power for 20 min. Next, a parylene layer was deposited by a LABCOATER2

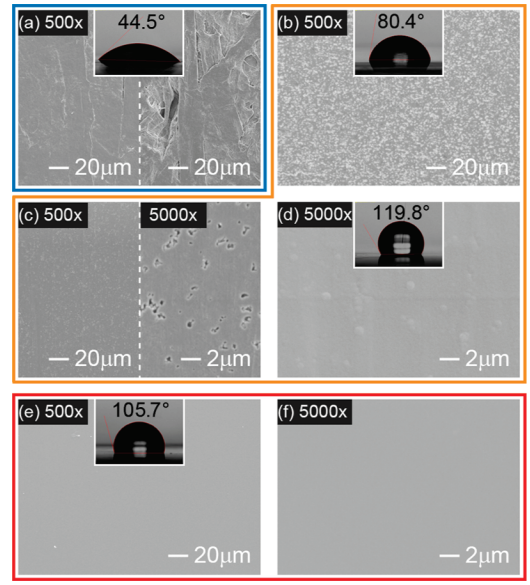

FIGURE 2. Surface morphology of paper substrates at different stages in the EW structure fabrication process: (a) as-received glassine; (b) as-received Kromekote; (c) Kromekote with a copper electrode layer; (d) Kromekote with a copper electrode layer and a parylene insulating layer; (e) as-received Sappi; (f) Sappi with an ITO electrode layer and a parylene insulating layer.

parylene deposition unit (PDS 2010, Specialty Coating Systems) at room temperature. Parylene layers of 1 and 0.5 μm were deposited using 0.8 and 0.4 g of starting material (Parylene C, Specialty Coating Systems). The operating pressure was less than 15 mTorr. The FluoroPel (PFC1601 V, Cytonix Corp.) hydrophobic insulator is a copolymer mixture of vinyl, perfluoropolyether, and urethane (with perfluoroalkyl groups) components. A 1 % FluoroPel solution in fluorosolvent was dip-coated, forming a ~150-nm film. After dip coating, the FluoroPel film was dried for 1 h at room temperature in air, producing a 16 mJ/m^2 surface energy (29). Subsequent annealing at 130 °C for 10 min improved the FluoroPel adhesion without damaging the underlying paper substrates. Dodecane oil was obtained from Acros Organics. For smooth EW operation, the surface tension (30) of the oil (25 mJ/m^2 for dodecane) should be higher than that of fluoropolymer (16 mJ/m^2 for FluoroPel) and lower than that of water (72 mJ/m^2). Viscosity is also an important factor to be considered. The viscosity (31–33) of dodecane (1.39 cP) is close to that of water (0.91 cP). If the oil is too viscous, the speed of the EW action will be compromised.

Scanning electron microscopy (SEM) and atomic force microscopy (AFM) were used to characterize the surface morphology. SEM (SX-40A, ISI) samples were prepared by depositing a thin layer of gold onto each paper substrate. AFM (Dimension Nanoscope IV, Veeco) scanning was performed in tapping mode. The CA was measured with the VCA Optima XE (Advanced Surface Technology) system. The paper device was immersed in an oil container, and a 3 μL DI water droplet was injected for CA measurement. The external bias was applied to the droplet through a wire connected to a function generator (AFG310, Tektronix) and a voltage amplifier (F10AD, FLC Electronics).

3. RESULTS AND DISCUSSION

The surface morphology of the starting paper substrates clearly influenced both the initial water CA and the CA versus voltage characteristics of the completed EW structures. Figure 2 contains SEM images of glassine, Kromekote, and Sappi paper substrates at different stages during the struc-

Table 2. Surface Roughness (nm) of Glass, Glassine, Kromekote, and Sappi Measured by AFM at Several Points in the EW Structure Fabrication Process

	glass	glassine	Kromekote	Sappi
starting substrate	<2	~300−400	42	2
after metal deposition[a]	3.8	~100−200	42	2.6
after insulator deposition[b]	4.9	~100−200	27	5.0

[a] 200 nm ITO (for glass and Sappi papers) or copper (for glassine and Kromekote papers). [b] 1 μm parylene.

ture fabrication process. The insets show a water droplet and its CA on the corresponding surface at each step. The CA was measured with the VCA Optima XE (Advanced Surface Technology) system. Parts a, b, and e of Figure 2 show SEM images of the starting papers. Typical features of the as-received surface of glassine are illustrated in Figure 2a. The photograph on the left-hand side of Figure 2a reveals a relatively smooth region, while on the right-hand side is shown a not infrequent very rough region. These smooth and rough regions are randomly located throughout the entire glassine surface. By comparison, the Kromekote paper shown at the same magnification in Figure 2b exhibits an array of small pores with less than 1 μm diameter. The pores have a fairly uniform distribution and no major defects were observed, making the starting surface of the Kromekote paper smoother than that of the glassine paper. The Sappi paper in Figure 2e shows the smoothest surface morphology, very close to that of a conventional glass substrate. The CAs of 5 μL DI water droplets on glassine (Figure 2a), Kromekote (Figure 2b), and Sappi (Figure 2e) papers are 44°, 80°, and 105°, respectively, indicating that glassine is strongly hydrophilic while Kromekote is only weakly hydrophilic and Sappi is adequately hydrophobic. The surface roughness of the glass and paper substrates was measured using AFM as layers were added in the fabrication process. The roughness results are summarized in Table 2. For glassine, the starting substrate exhibited a relatively large range of roughness values (~300−400 nm). After metal (200 nm copper) deposition and insulator (1 μm parylene) deposition, the roughness range is decreased (~100−200 nm), but a significant variation across the sample is still observed. The surface roughness of Kromekote was much superior to that of glassine, starting with an average of 42 nm for the as-received material and after metal deposition. The roughness decreased to an average of 27 nm after insulator deposition. SEM microphotographs of the Kromekote surface after metal and insulator deposition are shown in Figure 2c,d. The submicrometer pores seen in the high-magnification (5000×) microphotograph of Figure 2c after metal deposition have nearly disappeared after insulator deposition (Figure 2d). The inset in Figure 2d shows a 5 μL DI water droplet after hydrophobic coating (~150 nm FluoroPel) on the parylene surface. The CA increased from 80.4° to 119.8° after FluoroPel coating, which is sufficiently hydrophobic to observe EW operation. The surface roughness of the Sappi paper was the best (i.e., lowest) among the paper substrates investigated in this article. The roughness slightly increased

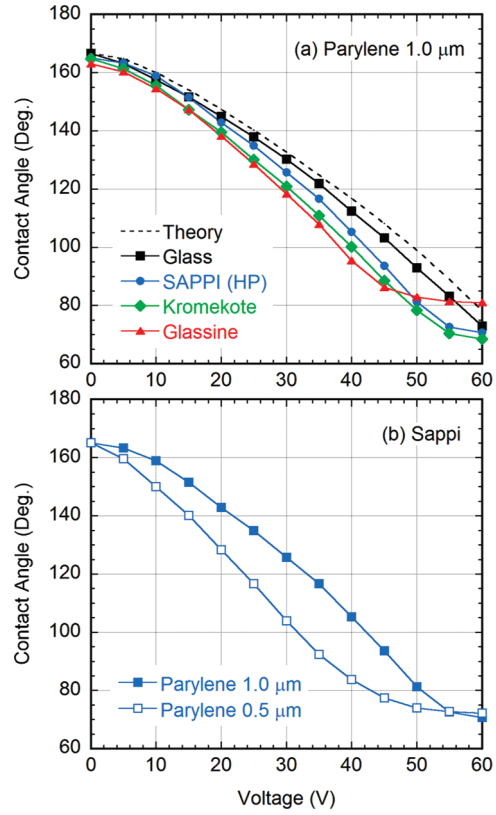

FIGURE 3. Water CA as a function of the dc voltage for EW devices on (a) glass and various paper substrates with a 1.0 μm parylene dielectric layer and (b) Sappi substrates with 0.5 and 1.0 μm parylene dielectric layers.

to 5 nm after ITO electrode and parylene deposition (Figure 2f) from 2 nm for the starting material (Figure 2e).

The EW effect was first evaluated by measuring the CA of DI water droplets immersed in dodecane oil as a function of the applied dc voltage. In general, the maximum voltage utilized was 60 V, in order to prevent dielectric breakdown, which for these devices typically occurred at ~70 V. Figure 3a shows the results of a water CA change on different paper substrates as a function of the applied voltage. As shown in Figure 3a, the initial CAs of 3 μL DI water droplets on the FluoroPel surface were nearly identical at ~165° for glassine, Kromekote, and Sappi paper EW devices. For comparison, the CA change of the EW device on a conventional glass substrate was also included. The CA of the glassine paper device with a 1-μm-thick parylene dielectric layer gradually decreased from 163° to 81° as the applied voltage was increased from 0 to 60 V. The CAs of the Kromekote and Sappi paper devices changed from 165° to 69° and from 165° to 71°, respectively, with the same applied voltage. The dotted line is the calculated CA from the Young−Lippmann relation (17), which describes the relationship between the CA (θ) and the applied voltage (V),

$$\cos\theta(V) = \cos\theta_0 + \frac{1}{2\gamma_{OW}}CV^2 = \cos\theta_0 + \frac{\varepsilon_0\varepsilon_r}{2\gamma_{OW}d}V^2$$

where θ_0 is the CA at zero bias, C is the capacitance per unit area, d is the insulator thickness, ε_0 is the permittivity in a

vacuum, ε_r is the relative dielectric constant of the insulator, γ_{OW} is the surface tension of the oil/water interface, and V is the voltage applied to the droplet. For many material systems used in EW structures, CA saturation is observed at higher voltages. The CA of the glassine paper device started to saturate at 45 V, while the CAs of the Kromekote and Sappi paper devices showed saturation from 55 V. However, the standard glass EW device did not show CA saturation up to 60 V. It is important to note that the glassine paper device exhibited a larger CA change than the other two paper devices and the glass EW device, prior to CA saturation. For example, at 40 V the CAs were 112°, 105°, 100°, and 96° for the glass, Sappi, Kromekote, and glassine substrates, respectively. The CA change with applied voltage is closely related to the surface roughness. As summarized in Table 2, the glassine paper has the highest surface roughness while the Sappi paper has the smoothest surface. The CA change (ΔCA) with voltage (before saturation) for the various substrates follows the same order as their respective surface roughness levels. This is consistent with a theoretical analysis (34) using the Wenzel model for two-fluid (oil/water) EW, which indicated that roughening the surface enhances the ΔCA in EW structures. A similar improvement in the CA with effective surface roughness has been experimentally obtained by Krupenkin et al. (35) using periodic nanopatterned posts. Interestingly, the rougher surface experiences CA saturation first. There are several potential mechanisms (charge trapping (36), droplet ejection (37) at the contact line, etc.) for CA saturation, and generally it has not been easy to pinpoint the specific cause in any one case. For the results presented here, it is likely that the CA saturation occurs at earlier voltages for rougher surfaces because the asperities on the surface form high-electric-field points that enhance charge trapping in the insulator.

Figure 3b shows the effect of the dielectric layer thickness on EW using Sappi paper substrates. Structures with 1.0- and 0.5-μm-thick parylene layers were utilized. For the Sappi substrate with 1 μm parylene, the ΔCA between zero bias and 40 V is 60°. For the thinner 0.5 μm parylene layer, the CA reaches 84° at 40 V (corresponding to ΔCA of 81°), as expected given (38) that a thinner dielectric layer produces a greater surface energy at a given voltage, resulting in a lower CA. Interestingly, both structures had the same CA (~70°) and ΔCA (~95°) at the highest bias value of 60 V. However, CA saturation begins to be observed at voltages >45 V.

Both dc and alternating-current (ac) biasing can be used to produce the EW effect. For ac biasing, a 0.1 M KCl solution was prepared instead of DI water and was also used for dc biasing to directly compare dc and ac EW effects. Figure 4 compares the CA change of a 3 μL droplet of a 0.1 M KCl solution in oil (dodecane) with dc and ac bias for EW devices on Sappi paper substrates with 1.0-μm-thick parylene layers. For an ac bias experiment, a 1 kHz square-wave signal was applied to a droplet and the equivalent root-mean-square (rms) values were used in Figure 4b. For dc bias (Figure 4a), the CA decreased from 165° to 72° (or a ΔCA of 93°) as

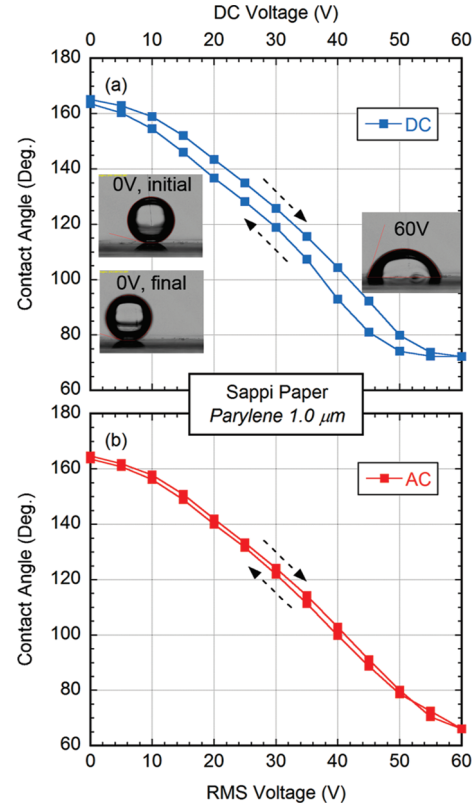

FIGURE 4. Water CA for EW devices with 1.0 μm parylene dielectric layers on Sappi substrates as a function of (a) the dc voltage [insets are photographs of a water/KCl droplet at initial conditions (0 V)], high voltage (60 V), and return to zero bias and (b) the rms voltage.

the voltage increased to 60 V. Reversing the direction of the voltage sweep, the CA recovered to 164°, which is essentially the initial CA. However, a relatively large hysteresis was observed at the larger voltage values (for example, a hysteresis of 11° at 40 V). The inserts in Figure 4a are photographs of a 3 μL droplet of 0.1 M KCl solution immersed in oil at the initial condition (0 V), at high voltage (60 V) and upon return to zero bias. For AC bias (Figure 4b), a ΔCA of 99° is obtained between zero bias and 60 V rms. This ΔCA is slightly higher than that obtained with DC bias. Furthermore, much less hysteresis was observed (with a maximum value of ~2°) for the ac bias mode. The decreased hysteresis and the increased ΔCA are the result of reduced charge injection into the fluoropolymer caused (39) by a time lag between the applied electric field and the motion of charges in the structure.

Because EW devices are repeatedly turned on and off in displays and other applications, the effect of bias cycling on the CA was investigated for the Sappi paper EW device. Figure 5 shows the CA modulation of a 3 μL droplet of a 0.1 M KCl solution in ambient oil obtained by switching the power supply between 0 and 50 V. Both dc and ac (1 kHz square wave) bias were utilized. The CA was measured for 10 sequential cycles. For the dc bias case, a decrease of 3.5° in ΔCA was observed between the first and second cycles. On the other hand, for the ac bias case, an initial ΔCA decrease of only 1.5° was observed. After this initial change, ΔCA stayed essentially constant for the remaining cycles for both dc and ac bias. This indicates that the EW operation

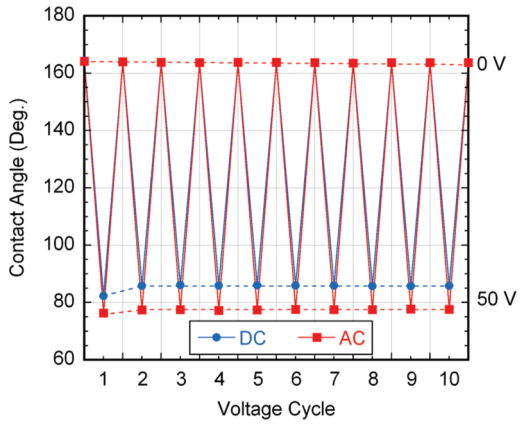

FIGURE 5. CA maxima (at 0 V) and minima (at 50 V) over 10 cycles for EW on Sappi substrates with a 1.0 μm parylene dielectric layer.

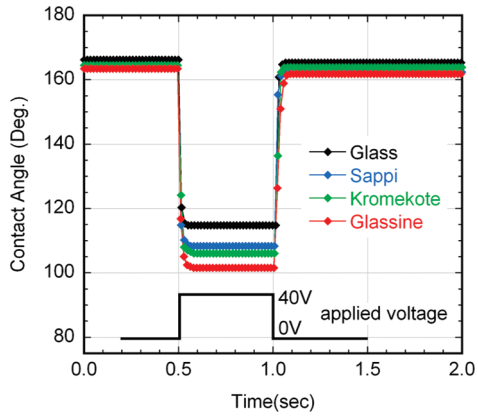

FIGURE 6. CA vs time during a 0.5 s voltage pulse for EW on several substrates: glass, Sappi, Kromekote, glassine; 1.0 μm parylene dielectric.

Table 3. Switching Times (ms) of EW Devices Fabricated on Glass, Glassine, Kromekote, and Sappi Substrates

	turn-on time	turn-off time
glass	15	17
glassine	28	40
Kromekote	28	29
Sappi	19	19

on paper substrates is stable with repeated motion of the water/oil boundary. This is an important consideration for the operation of EW-based displays and other applications.

The speed with which the water replaces oil under the influence of the applied voltage determines the speed of associated EW devices. The pulse response of glassine, Kromekote, and Sappi paper EW devices was measured to determine the switching time, as shown in Figure 6. For comparison, a conventional EW device built on a glass substrate with the same dielectric layers and thicknesses was also tested. A 40 V pulse of 500 ms duration and fast (2 ns) rise and fall times was applied to the 3 μL DI water droplet in oil. The CA was captured at 60 fps. The measured CA turn-on and turn-off times are summarized in Table 3. When the voltage changed from 0 to 40 V (*turn-on*), both glassine and Kromekote paper devices showed the same turn-on time of 28 ms, which is a factor of 2 slower than that for the conventional glass substrate EW device (15 ms). Changing the voltage from 40 to 0 V (*turn-off*) yielded switching times of 40 ms for glassine and 29 ms for the Kromekote device. The turn-off switching times for these paper devices were ~1.7−2.4 times slower than that of the glass substrate device (17 ms). This is not surprising given the surface roughness of glassine and Kromekote paper devices. The turn-on and turn-off switching times of the EW device on the Sappi paper were 19 ms, which is quite close to the EW switching speed of the glass substrate. This is not unexpected because the Sappi paper is nearly as smooth as the glass substrate.

4. CONCLUSION

EW operation on paper substrates has been demonstrated, indicating the feasibility of using paper as a cheap and flexible substrate for e-paper and other EW applications. The Sappi paper appears to be an excellent choice for paper-based EW devices because of its ultrasmooth surface, which leads to reduced CA hysteresis and saturation. The EW devices on Sappi substrates showed large CA modulation (~90°), which is more than sufficient for many EW applications. Their relatively fast switching speed (approximately a few tens of milliseconds) is very promising for video display applications.

Acknowledgment. This work was supported, in part, by a grant from the National Science Foundation (Grant ECCS-0725530). The authors greatly appreciate the material supplied by Sappi Ltd. The authors also appreciate useful technical discussions on EW with members of the Nanoelectronics Laboratory and Novel Devices Laboratory at the University of Cincinnati.

REFERENCES AND NOTES

(1) Roberts, J. C. *The Chemistry of Paper*; Royal Society of Chemistry: Cambridge, U.K., 1996.
(2) Martinez, A. W.; Phillips, S. T.; Whitesides, G. M. *Proc. Natl. Acad. Sci. U.S.A.* **2008**, *105*, 19606–19611.
(3) Bracher, P. J.; Gupta, M.; Mack, E. T.; Whitesides, G. M. *ACS Appl. Mater. Interfaces* **2009**, *1*, 1807–1812.
(4) Li, X.; Tian, J.; Nguyen, T.; Shen, W. *Anal. Chem.* **2008**, *80*, 9131–9134.
(5) Nystrom, G.; Razaq, A.; Stromme, M.; Nyholm, L.; Mihranyan, A. *Nano Lett.* **2009**, *9*, 3635–3639.
(6) Siegel, A. C.; Phillips, S. T.; Wiley, B. J.; Whitesides, G. M. *Lab Chip* **2009**, *9*, 2775–2781.
(7) Padki, S. *Packaging World* **2008**, 45–46.
(8) Ota, I.; Ohnishi, J.; Yoshiyama, M. *Proc. IEEE* **1973**, *61*, 832–836.
(9) Comiskey, B.; Albert, J. D.; Yoshizawa, H.; Jacobson, J. *Nature* **1998**, *394*, 253–255.
(10) Drzaic, P. *Nat. Photon.* **2009**, *3*, 248–249.
(11) Beni, G.; Hackwood, S. *Appl. Phys. Lett.* **1981**, *38*, 207–209.
(12) Seyrat, E.; Hayes, R. A. *J. Appl. Phys.* **2001**, *90*, 1383–1386.
(13) Roques-Carmes, T.; Hayes, R. A.; Feenstra, B. J.; Schlangen, L. J. M. *J. Appl. Phys.* **2004**, *95*, 4389–4396.
(14) Mugele, F.; Baret, J. C. *J. Phys.: Condens. Matter* **2005**, *17*, R705–R774.
(15) Girault, H. H. *Nat. Mater.* **2006**, *5*, 851–852.
(16) Shamai, R.; Andelman, D.; Berge, B.; Hayes, R. *Soft Matter* **2008**, *4*, 38–45.
(17) Quilliet, C.; Berge, B. *Curr. Opin. Colloid Interface Sci.* **2001**, *6*, 34–39.
(18) Hayes, R. A.; Feenstra, B. J. *Nature* **2003**, *425*, 383–385.
(19) Feenstra, B. J.; Hayes, R. A.; Camps, I. G. J.; Hage, L. M.; Johnson, M. T.; Roques-Carmes, T.; Schlangen, L. J. M.; Franklin, A. R.; Valdes, A. F.; Ford, R. A. *J. Soc. Info. Disp.* **2004**, *12*, 293–299.

(20) Heikenfeld, J.; Zhou, K.; Kreit, E.; Raj, B.; Yang, S.; Sun, B.; Milarcik, A.; Clapp, L.; Schwartz, R. *Nat. Photon.* **2009**, *3*, 292–296.
(21) Heikenfeld, J.; Steckl, A. J. *Appl. Phys. Lett.* **2005**, *86*, 151121–3.
(22) Gorman, C. B.; Biebuyck, H. A.; Whitesides, G. M. *Langmuir* **1995**, *11*, 2242–2246.
(23) Berge, B.; Peseux, J. *Eur. Phys. J. E* **2000**, *3*, 159–163.
(24) Kuiper, S.; Hendriks, B. H. W. *Appl. Phys. Lett.* **2004**, *85*, 1128–1130.
(25) Dong, L.; Agarwal, A. K.; Beebe, D. J.; Jiang, H. *Nature* **2006**, *442*, 551–554.
(26) Kim, D. Y.; Steckl, A. J. *Appl. Phys. Lett.* **2007**, *90*, 043507−3.
(27) Srinivasan, V.; Pamula, V. K.; Fair, R. B. *Anal. Chim. Acta* **2004**, *507*, 145–150.
(28) Son, S. U.; Garrell, R. L. *Lab Chip* **2009**, *9*, 2398–2401.
(29) Cytonix Corp., www.cytonix.com/fluoroproducts.html.
(30) Adamson, A. W.; Gast, A. P. *Physical Chemistry of Surfaces*; John Wiley & Sons, Inc.: New York, 1997.
(31) Yaws, C. L. *Handbook of Viscosity*; Gulf Publishing Co.: Houston, TX, 1995; Vol. 1.
(32) Yaws, C. L. *Handbook of Viscosity*; Gulf Publishing Co.: Houston, TX, 1995; Vol. 2.
(33) Yaws, C. L. *Handbook of Viscosity*; Gulf Publishing Co.: Houston, TX, 1995; Vol. 3.
(34) Sureshkumar, P.; Kim, M.; Song, E. G.; Lim, Y. J.; Lee, S. H. *Surf. Rev. Lett.* **2009**, *16*, 23–28.
(35) Krupenkin, T. N.; Taylor, J. A.; Schneider, T. M.; Yang, S. *Langmuir* **2004**, *20*, 3824–3827.
(36) Verheijen, H. J. J.; Prins, M. W. J. *Langmuir* **1999**, *15*, 6616–6620.
(37) Vallet, M.; Vallade, M.; Berge, B. *Eur. Phys. J. B* **1999**, *11*, 583–591.
(38) Moon, H.; Cho, S. K.; Garrell, R. L.; Kim, C. J. *J. Appl. Phys.* **2002**, *92*, 4080–4087.
(39) Quinn, A.; Sedev, R.; Ralston, J. *J. Phys. Chem. B* **2005**, *109*, 6268–6275.

AM100757G